Tech Science Press

Fractional-Order Control of a Wind Turbine Using Manta Ray Foraging Optimization

Hegazy Rezk[1,2,*], Mohammed Mazen Alhato[3], Mohemmed Alhaider[1] and Soufiene Bouallègue[3,4]

[1]College of Engineering at Wadi Addawaser, Prince Sattam Bin Abdulaziz University, Al-Kharj, 11911, Saudi Arabia
[2]Department of Electrical Engineering, Faculty of Engineering, Minia University, 61517, Minia, Egypt
[3]Research Laboratory in Automatic Control (LARA), National Engineering School of Tunis (ENIT),
University of Tunis, Tunis, 1002, Tunisia
[4]High Institute of Industrial Systems of Gabès, University of Gabès, Gabès, 6011, Tunisia
[*]Corresponding Author: Hegazy Rezk. Email: hr.hussien@psau.edu.sa
Received: 22 December 2020; Accepted: 25 January 2021

Abstract: In this research paper, an improved strategy to enhance the performance of the DC-link voltage loop regulation in a Doubly Fed Induction Generator (DFIG) based wind energy system has been proposed. The proposed strategy used the robust Fractional-Order (FO) Proportional-Integral (PI) control technique. The FOPI control contains a non-integer order which is preferred over the integer-order control owing to its benefits. It offers extra flexibility in design and demonstrates superior outcomes such as high robustness and effectiveness. The optimal gains of the FOPI controller have been determined using a recent Manta Ray Foraging Optimization (MRFO) algorithm. During the optimization process, the FOPI controller's parameters are assigned to be the decision variables whereas the objective function is the error racking that to be minimized. To prove the superiority of the MRFO algorithm, an empirical comparison study with the homologous particle swarm optimization and genetic algorithm is achieved. The obtained results proved the superiority of the introduced strategy in tracking and control performances against various conditions such as voltage dips and wind speed variation.

Keywords: Renewable energy; modeling; wind turbine; doubly fed induction generator; fractional order control; manta ray foraging optimization

1 Introduction

Recently, the utilization of renewable energy sources has prompted the reduction of conventional fossil-fuel energy source dependency. Wind energy as a renewable source has gained considerable attention because it is clean and pollution-free. Wind Energy Conversion Systems (WECSs) are mainly based on Wind Turbines (WTs). However, the intensive research that is executed in the wind technology market produced various wind energy configurations. The most popular configuration is the Doubly Fed Induction Generator (DFIG) linked with the WTs [1,2]. This type is vastly used due to its considerable advantages, which the decoupled control of active

and reactive powers, low converters' costs, and mechanical exertion decrease are the main ones. The DFIG is linked to the grid via a converter consisting of a Rotor Side Converter (RSC) and a Grid Side Converter (GSC). This topology enables the converter to catch the portion of 20% to 30% of the overall power resulting in reducing its cost [3,4].

Several research works have assured to reinforce the efficiency of WECSs. Among the existing control strategies, the classical Vector Control (VC) is broadly applied. This scheme allows independent control of the power components exchanging between the DFIG and the grid and keeps the DC-link voltage constant. The VC method is mostly attained by regulating the decoupled rotor converter currents using linear Proportional-Integral (PI) controllers [5,6]. The major disadvantage of this scheme is that the effectiveness of the DFIG relies on the accurate adjusting of the PI parameters and the exact values of DFIG parameters such as stator resistance, rotor resistance, and inductances [7]. Hence, the PI controllers-based VC method provides poor performance and low robustness when actual DFIG parameters deviate from the nominal values, which have been used in the control system [8].

In this regard, to outperform the drawbacks of the classical VC method based, various control structures are proposed to improve the dynamic response [9]. Therefore, the Fractional-Order (FO) PI controllers emerge as a relevant option, as demonstrated by several applications. This type of controller combines the benefits of the classical PI and fractional calculus. Therefore, this leads to better performance [10,11]. Applying a FOPI controller in the pitch angle control loop and is compared with a fuzzy PI controller has been suggested in [12]. In [13], the authors focused on attenuating the Total Harmonic Distortion (THD) value in the voltage and current signals using the FOPI controllers in the back-to-back converter. However, the design approach was not indicated. Besides, a simple wind speed profile with fixed step changes is investigated. Another solution adopting the FOPI scheme has been discussed for the active power control based DFIG in [14]. Besides, the FOPI controllers are applied in the internal loop of rotor current instead of the classical PI controllers. Also, the tuning of the FOPI controllers is executed using the frequency domain specifications. All these studies discussed the FOPI method in the presence of the L-filter at the GSC.

In this work, the FOPI controller is designed for the DC-link voltage loop in the presence of the LCL filter. This filter leads to improve the THD of the current grids [15]. Usually, the FOPI controllers have an extra adjustable parameter than the classical PI controllers. This parameter makes the controller design more complicated. Many methods are adopted for the tuning of FOPI controllers. However, most of these methods depend on the trial-errors procedure and the frequency domain specifications. However, since the FOPI controller gains rely on the mathematical representation, the control schemes become prone to error. Besides, the tuning process can be time-consuming, and the optimal gains may not be caught. To this end, the nature-inspired meta-heuristics such as Particle Swarm Optimization (PSO) and Genetic Algorithm (GA) are applied [16–18]. Therefore, this work uses a Manta Ray Foraging Optimization (MRFO) algorithm to attain the FOPI controller gains' [19]. The main contributions of the proposed FOPI controller are: (1) It ensures high tracking performance through the selection of the optimal gains for the FOPI controller by using the recent metaheuristic MRFO algorithm. (2) It presents a fast dynamic behavior and high robustness of the closed-loop DC-link voltage loop under external disturbances such as wind speed variation and the voltage dip conditions. (3) It reduces the values of the THD of the grid currents more than the traditional PI controller.

The remainder of this paper is organized as follows. The mathematical model of DFIG based WT is detailed in Section 2. In Section 3, the description of the FOPI controller for the DC-link

voltage dynamics is analyzed. Also, such an MRFO algorithm is described and given. Section 4 states the implementation of the proposed MRFO-tuned FOPI control approach. Concluding remarks are given in Section 5.

2 Modelling of the DFIG Based Wind Energy Converter

2.1 Modelling of the Wind Turbine

The rotor blade of the WT is responsible for catching the wind power and converting it into kinetic energy. The captured mechanical power is given as follows [2,3]:

$$P_m = \frac{1}{2}\rho C_p(\lambda, \beta)\pi R^2 V_w^3 \tag{1}$$

where ρ is the air density, C_p is the power coefficient that depends on both the tip-speed ratio λ and the blade pitch angle β, R is the turbine radius and V_w is the wind speed.

The tip-speed ratio is defined as the ratio of the blade tip-speed to the wind speed. It is given by:

$$\lambda = \frac{\Omega_t R}{V_w} \tag{2}$$

where Ω_t is the angular speed of the WT.

2.2 Modelling of the DFIG

The dynamic equations of the DFIG model can be expressed as [2,3]:

$$\begin{cases} V_{ds} = R_s i_{ds} + \dfrac{d\varphi_{ds}}{dt} - \omega_s \varphi_{qs} \\[2mm] V_{qs} = R_s i_{qs} + \dfrac{d\varphi_{qs}}{dt} + \omega_s \varphi_{ds} \\[2mm] V_{dr} = R_r i_{dr} + \dfrac{d\varphi_{dr}}{dt} - (\omega_s - \omega_m)\varphi_{qr} \\[2mm] V_{qr} = R_r i_{qr} + \dfrac{d\varphi_{qr}}{dt} + (\omega_s - \omega_m)\varphi_{dr} \end{cases} \text{ and } \begin{cases} \varphi_{ds} = L_s i_{ds} + L_m i_{dr} \\[2mm] \varphi_{qs} = L_s i_{qs} + L_m i_{qr} \\[2mm] \varphi_{dr} = L_r i_{dr} + L_m i_{ds} \\[2mm] \varphi_{qr} = L_r i_{qr} + L_m i_{qs} \end{cases} \tag{3}$$

where V_s and i_s are the stator voltage and current, V_r and i_r are the rotor voltage and current, φ_s and φ_r are the stator and rotor flux linkages, R_s and R_r are the stator and rotor resistances, ω_s and ω_m are the stator and rotor angular frequencies, respectively. The subscripts d and q denote the direct and quadrature axis components, respectively.

In this work, the Stator Flux Orientation (SFO) is adopted to implement the power control of the DFIG. Supposing that the electrical grid is stable, the stator flux is constant. Hence, according to the above presumptions, the stator voltages and fluxes can be written as follows [3]:

$$\begin{cases} V_{ds} = 0 \\ V_{qs} = V_s = \omega_s \varphi_{ds} \end{cases}, \text{ and } \begin{cases} \varphi_{ds} = \varphi_{ds} = L_s i_{ds} + L_m i_{dr} \\ \varphi_{qs} = 0 = L_r i_{qs} + L_m i_{qr} \end{cases} \tag{4}$$

where L_s, L_r, and L_m are the stator, rotor, and magnetizing inductances, respectively.

The stator power components and rotor voltages are expressed as [3,4]:

$$\begin{cases} P_s = \dfrac{3}{2}\left(V_{ds}i_{ds}+V_{qs}i_{qs}\right)=-\dfrac{3}{2}\dfrac{L_m}{L_s}V_s i_{qr} \\[3mm] Q_s = \dfrac{3}{2}\left(V_{qs}i_{ds}+V_{ds}i_{qs}\right)=\dfrac{3}{2}\left(\dfrac{V_s^2}{\omega_s L_s}-\dfrac{L_m}{L_s}V_s i_{dr}\right) \end{cases} \tag{5}$$

$$\begin{cases} V_{dr}=R_r i_{dr}+\sigma L_r \dfrac{di_{dr}}{dt}-\sigma \omega_r L_r i_{qr} \\[3mm] V_{qr}=R_r i_{qr}+\sigma L_r \dfrac{di_{qr}}{dt}+\sigma \omega_r L_r i_{dr}+\dfrac{L_m}{L_s}\omega_r \varphi_{ds} \end{cases} \tag{6}$$

where $\sigma = L_r - L_m^2/L_s$ and $\omega_r = \omega_s - \omega_m$.

2.3 Modelling of the GSC and the DC-Link Circuits

The GSC is connected to the grid through an LCL-filter. However, for better understanding the control of the GSC, it is necessary to describe the model of the grid side system and DC-link parts. The mathematical formulation of the GSC in the dq synchronous frame is defined by Eq. (7). The term L_T represents the sum of the converter L_i and grid side L_g inductances. In fact, the LCL-filter can be approximated to an L-filter equal to the sum of the LCL-filter inductors [2]:

$$\begin{cases} L_T \dfrac{di_{gd}}{dt}=-R_T i_{gd}+\omega_g L_T i_{gq}+e_{gd}-V_{df} \\[3mm] L_T \dfrac{di_{gq}}{dt}=-R_T i_{gq}-\omega_g L_T i_{gd}+e_{gq}-V_{qf} \end{cases} \tag{7}$$

where V_{df} and V_{qf} are the terms of the power-converter side voltage, i_{gd} and i_{gq} are the terms of the grid currents, e_{gd} and e_{gq} are the terms of the grid voltage, and R_T is the sum of the converter and grid side resistors.

The DC-link circuit, which connects the GSC and RSC components, can be modeled as follows [2,9]:

$$\frac{dV_{dc}}{dt}=\frac{1}{C_{dc}}\left(\frac{3}{2}\frac{e_{dg}}{V_{dc}}i_{dg}-i_{rdc}\right) \tag{8}$$

where C_{dc} is the DC-link capacitance and i_{rdc} is the current flowing between the DFIG rotor and the DC-link. From the voltage dynamics described by Eq. (8), the DC-link voltage can be regulated via the direct grid current.

3 Control Strategy and Optimization

3.1 Problem Statement

Generally, the classical vector control of the DFIG system is divided into the RSC and GSC control diagrams, which the PI controllers are usually used in this control scheme. The RSC is adopted to regulate the stator power components. On the other hand, the GSC is adopted to maintain the DC-link voltage constant. In this work, the FOPI controller is applied in the GSC circuit to improve its control performance. As a result, the excellent tracking performance, the reduced chattering, and the robustness of the DC-link under disturbances are improved. However, a good selection of the FOPI controller gains is a big challenge, where the optimal parameters

improve the system performance. Control parameter tuning using the conventional manual trials-and-errors based approach is a time-consuming and non-systematic procedure. The manta ray foraging optimization is proposed to improve the selection of the FOPI regulator gains. The proposed FOPI based DC-link voltage for the DFIG control scheme is shown in Fig. 1.
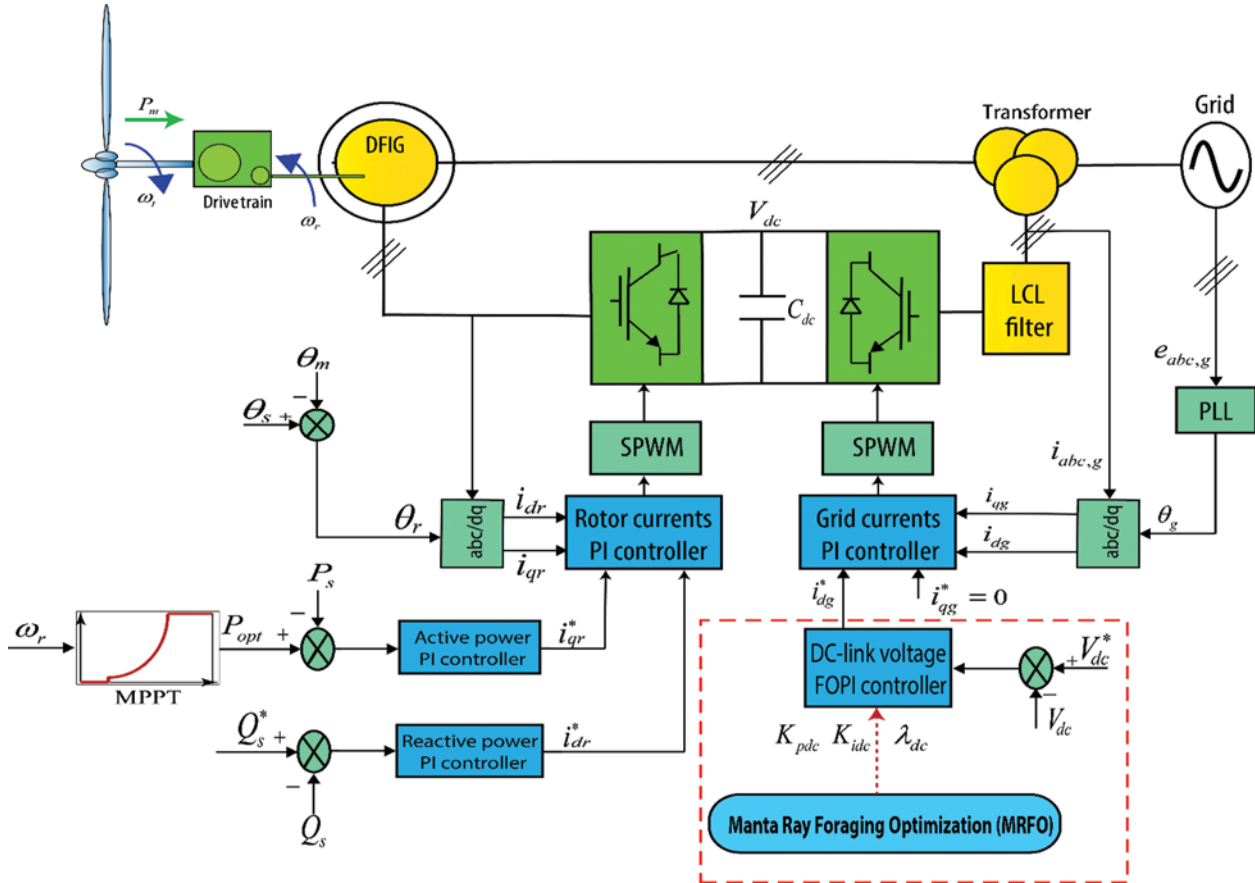

**Figure 1:** The proposed control approach applied to the DFIG system

3.2 Fractional-Order PI Controller

Fractional-Order (FO) controllers gained great attention and high penetration in many applications. Presently, many researchers tried to achieve the most reliable performance of such controllers [11]. Fractional-Order Proportional-Integral-Derivative (FOPID) controller was firstly presented in [20]. It is characterized by better performance than the conventional PID one, especially for the closed-loop control process. Five parameters are required to model the $PI^{\lambda}D^{\mu}$ controllers which are the gains of PID (K_p, K_i, and K_d), the order of integrator (λ), and the order of derivative (μ). Fig. 2 shows the block diagram of the $PI^{\lambda}D^{\mu}$ controller with a plant.

Referring to Fig. 2, the transfer function of the FOPID controller can be written in the following form:

$$G_c(s) = \frac{U(s)}{E(s)} = K_p + K_i s^{-\lambda} + K_d s^{\mu} \quad \lambda, \mu > 0 \tag{9}$$

where $U(s)$ and $E(s)$ are the output and input of the FOPID in the s-domain, respectively.
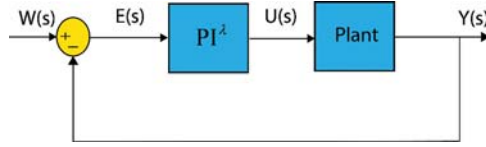
Figure 2: Block diagram of the PI$^\lambda$ controller with a plant

The output of the PI$^\lambda$D$^\mu$ controller in the continuous-time framework can be written as follows:

$$u(t) = K_p e(t) + K_i D^{-\lambda} e(t) + K_d D^{-\mu} e(t) \tag{10}$$

The main object of the FOPI controller is to feed the plant with the desired input via minimizing the error signal fed to it (i.e., E(s) controller's input). This can be achieved when the parameters of the PI$^\lambda$ controller are tuned in a correct manner.

The parameter λ gives more flexibility to enhance the FOPI performance better than the conventional PI. However, many previous works performed the tuning process of the PI$^\lambda$D$^\mu$ controller, which is considered a big challenge for most researchers [21]. In this work, the MRFO approach is selected to identify the optimal parameters of PI$^\lambda$ controller for the DC-link voltage loop, which the tuning problem associated with the PI$^\lambda$ controller, is formulated as a constrained optimization problem.

Several time-domain performance metrics, i.e., maximum overshoot, steady-state error, rise, and/or settling times can be used as operational constraints for the formulated optimization problem. Such a problem deals to minimize a set of the well-known performance criteria such as Integral Absolute Error (IAE), Integral of Square Error (ISE), and Root Square Mean Error (RSME) as follows:

$$\begin{cases} \text{minimize } J_m(\boldsymbol{x}, t), \, m \in \{IAE, ISE, RSME\} \\[4pt] \boldsymbol{x} = \left[K_{pdc}, K_{idc}, \lambda_{dc}\right]^T \in \boldsymbol{S} \subseteq \mathbb{R}_+^3 \\[4pt] \text{subject to:} \\[4pt] g_1(\boldsymbol{x}, t) = \delta_{dc} - \delta_{dc}^{\max} \leq 0 \\[4pt] K_{pdc,\min} \leq K_{pdc} \leq K_{pdc,\max} \\[4pt] K_{idc,\min} \leq K_{idc} \leq K_{idc,\max} \\[4pt] \lambda_{dc,\min} \leq \lambda_{dc} \leq \lambda_{dc,\max} \end{cases} \tag{11}$$

where $J_m: \mathbb{R}_+^3 \to \mathbb{R}$ are the cost functions, $g_q: \mathbb{R}_+^3 \to \mathbb{R}$ are the problem's inequality constraints, δ_{dc} and $\delta_{dc}^{\max}$ are the overshoot and specified maximum overshoot of the DC-link voltage step response, respectively. The terms $K_{pdc}, K_{idc}, \lambda_{dc}$ indicate the gains of the PI$^\lambda$ controller for the DC-link voltage control loop. Fig. 3 gives the optimization-based tuning scheme of the FOPI controller for the DC-link voltage control.
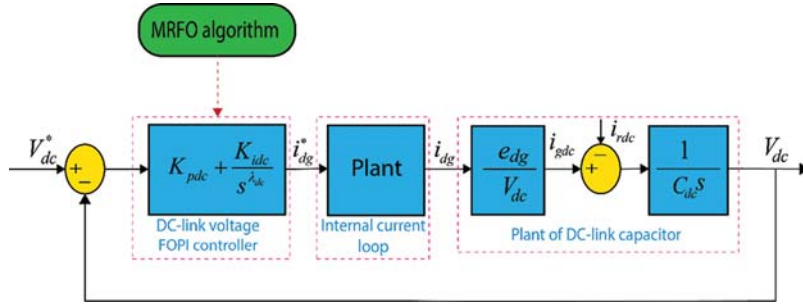
Figure 3: FOPI control scheme for the DC-link voltage based MRFO algorithm

3.3 Manta Ray Foraging Optimization

Manta rays are fancy creatures although they appear to be terrible. They are one of the largest known marine creatures. MRFO is recently suggested by Zhao et al. [19]. It is inspired by three foraging behaviors including chain foraging, cyclone foraging, and somersault foraging. The mathematical models are clearly described in [19]. During the chain foraging, manta rays line up head to tail and form a foraging chain. The individuals update their positions based on the following relations:

$$x_i^d(t+1) = \begin{cases} x_i^d(t) + r\left(x_{best}^d(t) - x_i^d(t)\right) + \alpha\left(x_{best}^d(t) - x_i^d(t)\right), & i = 1 \\ x_i^d(t) + r\left(x_{i-1}^d(t) - x_i^d(t)\right) + \alpha\left(x_{best}^d(t) - x_i^d(t)\right), & i = 2, \ldots, N \end{cases} \tag{12}$$

$$\alpha = 2r\sqrt{|\log(r)|} \tag{13}$$

where $x_i^d(t)$ is the position of the ith individual at time t in the dth dimension, r denotes a random number [0 1], α is a weight coefficient and $x_{best}^d(t)$ denotes the plankton with high concentration.

When a school of manta rays recognizes a patch of plankton in deep water, they will form a long foraging chain and swim towards the food by a spiral. The following mathematical relation can be used to simulate the spiral-shaped movement of manta rays in 2-D space:

$$\begin{cases} X_i(t+1) = X_{best} + r(X_{i-1}(t) - X_i(t)) + e^{b\omega}\cos(2\pi\omega)(X_{best} - X_i(t)) \\ Y_i(t+1) = Y_{best} + r(Y_{i-1}(t) - Y_i(t)) + e^{b\omega}\sin(2\pi\omega)(Y_{best} - Y_i(t)) \end{cases} \tag{14}$$

where ω is a random value.

This motion behavior can be extended to an n-D space. For simplicity, the model of cyclone foraging can be represented using the following relations:

$$x_i^d(t+1) = \begin{cases} x_{best}^d + r\left(x_{best}^d(t) - x_i^d(t)\right) + \beta\left(x_{best}^d(t) - x_i^d(t)\right), & i = 1 \\ x_{best}^d + r\left(x_{i-1}^d(t) - x_i^d(t)\right) + \beta\left(x_{best}^d(t) - x_i^d(t)\right), & i = 2, \ldots, N \end{cases} \tag{15}$$

$$\beta = 2e^{r_1\frac{T-t+1}{T}}\sin(2\pi r_1) \tag{16}$$

where β denotes a weight coefficient, T is the maximum number of iterations and r_1 is a random value [0 1].

Then, every individual search for a new position far from the current best one by assigning a new random position as following:

$$x^d_{rand} = Lb^d + r \left(Ub^d - Lb^d \right) \tag{17}$$

$$x^d_i(t+1) = \begin{cases} x^d_{rand} + r \left(x^d_{rand} - x^d_i(t) \right) + \beta \left(x^d_{rand}(t) - x^d_i(t) \right), & i = 1 \\ x^d_{rand} + r \left(x^d_{i-1}(t) - x^d_i(t) \right) + \beta \left(x^d_{rand}(t) - x^d_i(t) \right), & i = 2, \dots, N \end{cases} \tag{18}$$

where Lb^d and Ub^d are the lower and upper limits

Lastly, in the somersault foraging, the position of the food is viewed as a pivot. Each individual tends to swim to and from around the pivot and somersault to a new location. The following relation can be representing this stage:

$$x^d_i(t+1) = x^d_i(t) + S \left(r_2 x^d_{best} - r_3 x^d_i(t) \right), \quad i = 1, \dots, N \tag{19}$$

where S denotes the somersault factor, $S = 2$, r_2, and r_3 are random values.

4 Results and Discussion

This section investigates the numerical simulations executed to assess the effectiveness of the proposed MRFO-tuned FOPI controller design approach for the studied DFIG. The demonstrative control results of the active/reactive powers and DC-link voltage are discussed and analyzed. The parameters of the used DFIG system are presented in [2]. To investigate the performance of the proposed algorithm, GA and PSO algorithms are implemented, in which the number of the population size is 10, and the maximum number of iterations is 25.

Tab. 1 lists the optimization results of the problem (11). It can be clearly observed that the proposed MRFO algorithm produces the best mean solutions over the three used indices in comparison with the other algorithms. Fig. 4 shows the convergence history of the mean cost functions for the RMSE index. The MRFO algorithm outperforms the compared algorithms in terms of fastness and non-premature convergence. The Box-and-Whisker plots of the mean objective function values are presented in Fig. 5. The results of the cost function prove the superiority of the proposed MRFO algorithm. Hence, the parameters of the FOPI controller-based MRFO optimization algorithm are adopted. The active/reactive powers, DC-link voltage, and THD of the grid currents are displayed to prove the performance of the proposed FOPI controller. The demonstrative results of the FOPI controller are tested under the following conditions: (1) Variations in the DC-link reference. (2) Wind speed step variation. (3) Voltage dips conditions.
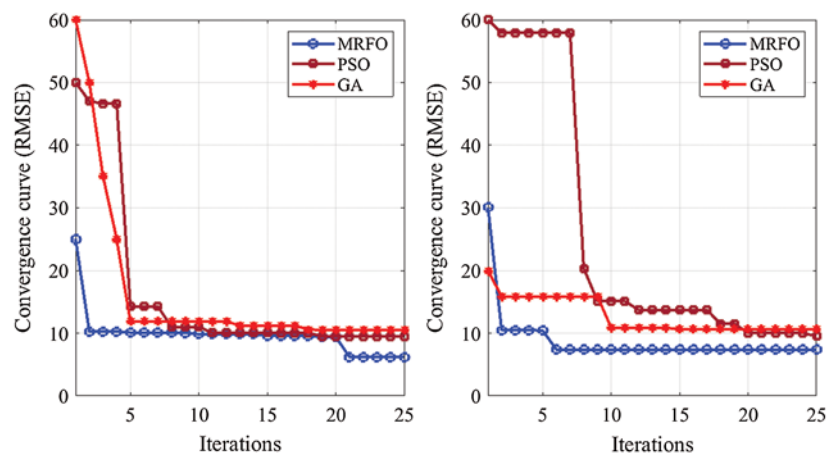
4.1 DC-link Voltage Step Change

Fig. 6 illustrates the dynamic performance of the DC-link voltage control. From Tab. 2, it can be observed that the FOPI controller introduces the best time domain performances in terms of settling time, rise time, and overshoot minimization. Besides, it can be noted that the proposed controller reduces the chattering effect in comparison with the PI controller.

**Table 1:** Statistical results of optimization for the problem (11) over 30 independent runs

Indices		PSO	GA	MRFO
IAE	Best	7.407	10.360	7.413
	Mean	176.481	275.186	**9.296**
	Worst	2478.336	2415.689	12.572
	STD	625.733	725.189	1.049
ISE	Best	51.308	54.190	53.213
	Mean	18493.80	822.479	**146.786**
	Worst	275116.6	1743.878	177.634
	STD	69739.25	447.127	46.236
RMSE	Best	6.158	6.185	6.224
	Mean	75.585	114.878	**9.142**
	Worst	998.160	991.073	9.993
	STD	250.784	296.306	1.032

Figure 4: Convergence histories of the optimization algorithms: RMSE index
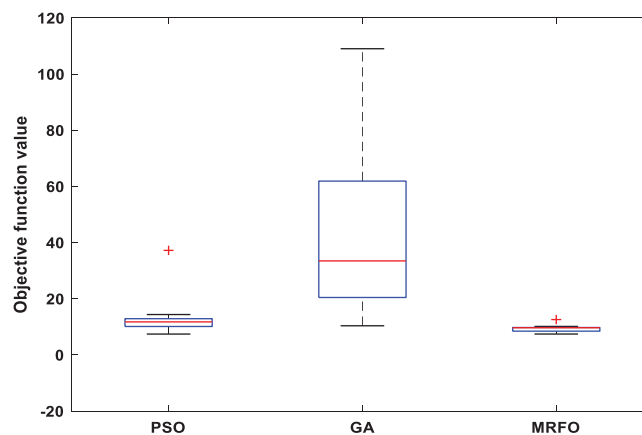
**Figure 5:** Box-and-Whisker plot of the optimization algorithms: RMSE index
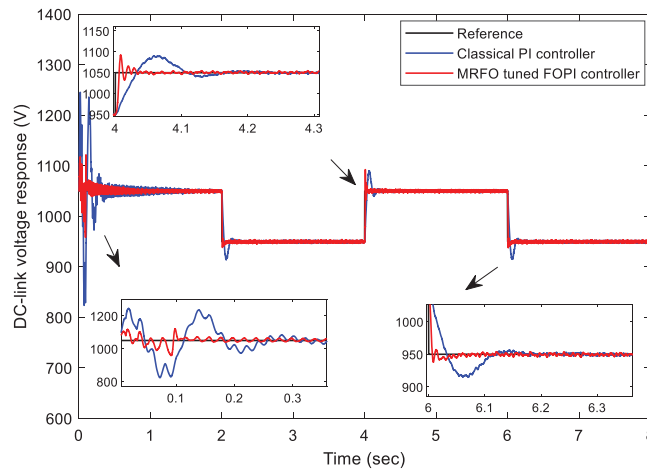
**Figure 6:** Performance comparison of the DC-link voltage under step changes

Table 2: Time-domain performances' comparison for the DC-link voltage dynamics

Control strategies	t_r (sec)	t_s (sec)	δ (%)
Classical PI controller	0.026	4.16	3.8
MRFO-tuned FOPI controller	0.003	4.03	4.1

Fig. 7 shows the dynamic performance of the reactive power response. It can be noted that the decoupling between the active and reactive powers is ensured. Fig. 8 shows the THD of the grid currents for the two control strategies, which this result confirms that the proposed FOPI controller further attenuates the harmonics of the grid currents.
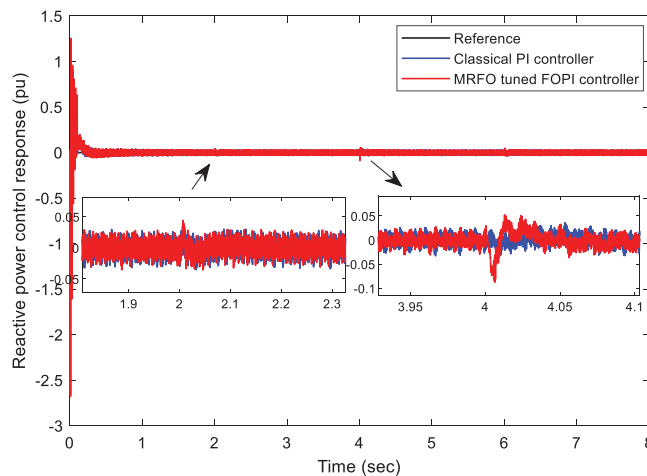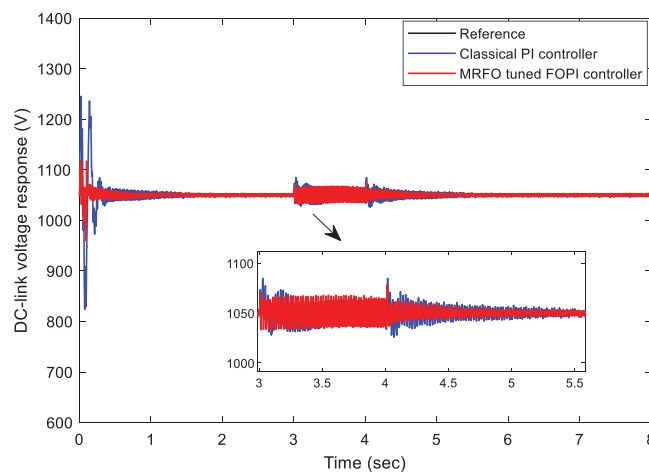

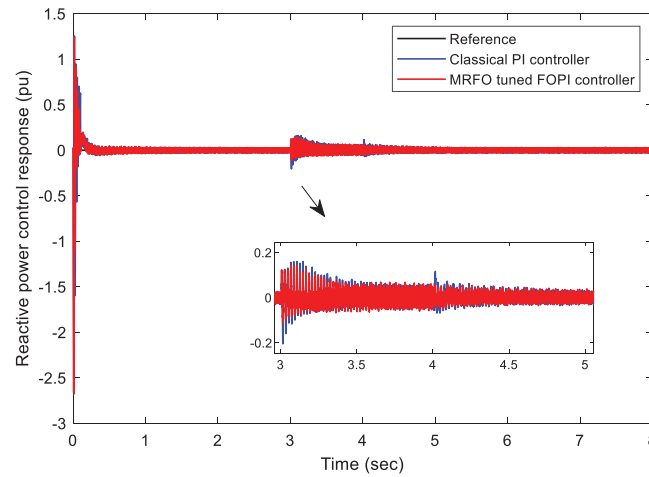**Figure 7:** Performance comparison of the stator reactive power under step changes
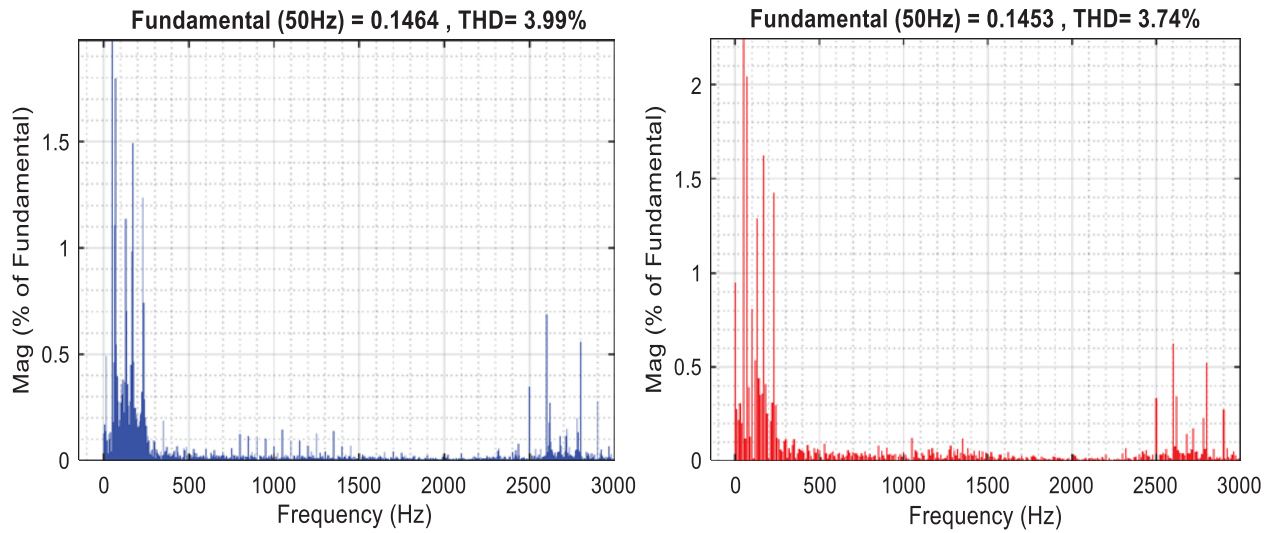
Figure 8: Grid current harmonic spectra: (a) PI controller; (b) FOPI controller

4.2 Voltage Dip Condition

To investigate the performance of the proposed controller, the MRFO-based PI^λ robustness is examined under the dip voltage scenario. A 30% voltage drop is considered at the simulation times 3 and 4 s. The dynamic responses of the FOPI and PI controllers are presented in Figs. 9 and 10, respectively. It can be observed that the proposed control method can successfully mitigate the voltage dip, in which the fluctuations in the DC-link and the stator reactive power during the voltage dips are relatively small. This result confirms the robustness of the proposed FOPI controller-based MRFO.
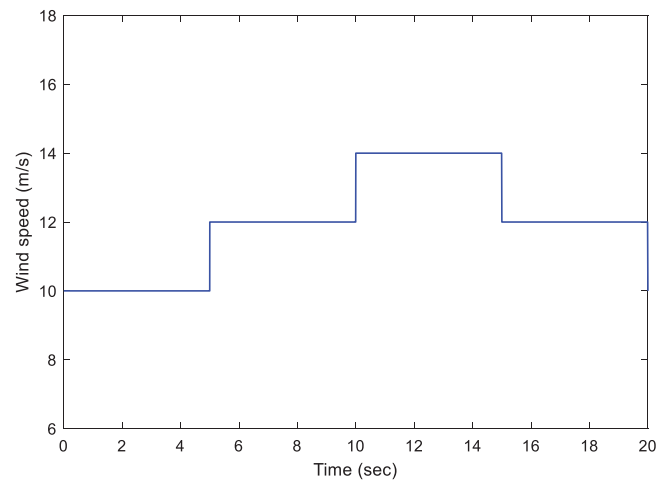

Figure 9: Performance comparison of the DC-link voltage under the voltage dip condition
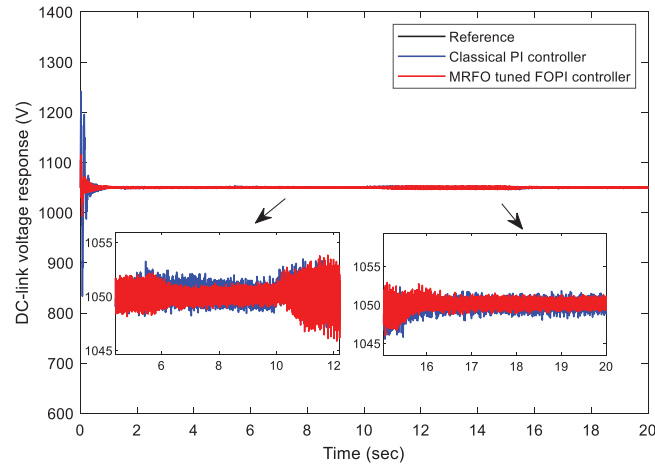
Figure 10: Performance comparison of the stator reactive power under the voltage dip condition
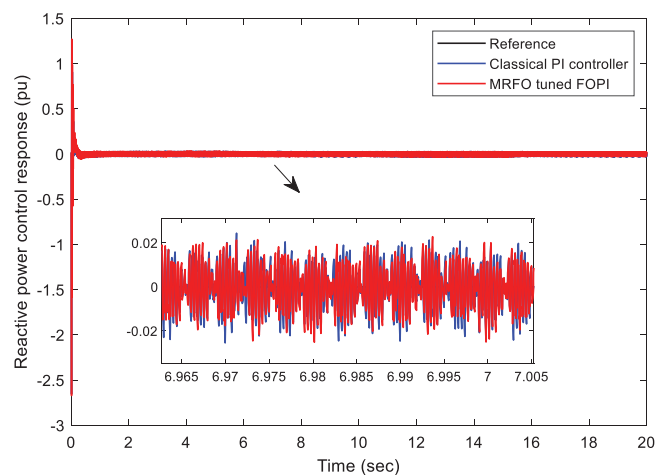
4.3 Wind Speed Step Variation

The step variation scenario is considered for wind speed to appraise the tracking performance of the understudy controllers. This scenario is presented in Fig. 11. Besides, Figs. 12 and 13 show the simulation results which confirm the efficiency of the MRFO-tuned FOPI. These MRFO-based PI^λ closed-loop responses can accurately track the reference values with low fluctuations compared to the classical PI one.

Figure 11: Wind speed step variation between 10 and 14 m/s

Figure 12: Performance comparison of the DC-link voltage under the wind speed step variation

Figure 13: Performance comparison of the stator reactive power under the wind speed step variation

5 Conclusions

This research work compares the classical PI and FOPI controllers in a DFIG-based WT. The gains of the FOPI are acquired by using the MFRO meta-heuristic algorithm. The obtained results show that the FOPI controller performs better than the traditional PI in the DC-link voltage dynamics. (1) The FOPI-tuned MRFO controller needs a lower rise time and settling time, less tuning time, and better robustness with wind speed variations and voltage dip conditions. (2) The FOPI controller enhances remarkably the start-up performance and makes the system reach its steady-state region without a considerable impact. The gained results show that the proposed FOPI controller tuned-MRFO method is a promising alternative strategy for controlling the DFIG system by systematically tuning the unknown FOPI controllers' parameters efficiently.

Conflicts of Interest: The authors declare that they have no conflicts of interest to report regarding the present study.

References

[1] K. A. Naik, C. P. Gupta and E. Fernandez, "Design and implementation of interval type-2 fuzzy logic-PI based adaptive controller for DFIG based wind energy system," *International Journal of Electrical Power & Energy Systems*, vol. 115, no. 1, pp. 1–16, 2020.

[2] M. M. Alhato, S. Bouallègue and H. Rezk, "Performance improvement of direct power control of doubly fed induction generator based wind turbine through second-order sliding mode control approach," *Mathematics*, vol. 8, no. 11, pp. 1–31, 2020.

[3] M. M. Alhato and S. Bouallègue, "Direct power control optimization for doubly fed induction generator based wind turbine systems," *Mathematical and Computational Applications*, vol. 24, no. 3, pp. 1–27, 2019.

[4] B. Hamane, M. L. Doumbia, M. Bouhamida, A. Draou, H. Chaoui *et al.,* "Comparative study of PI, RST, sliding mode and fuzzy supervisory controllers for DFIG based wind energy conversion system," *International Journal of Renewable Energy Research*, vol. 5, no. 4, pp. 1174–1185, 2015.

[5] R. Pena, J. C. Clare and G. M. Asher, "Doubly fed induction generator using back-to-back PWM converters and its application to variable-speed wind-energy generation," *IEE Proc. Electric Power Applications*, vol. 143, no. 3, pp. 231–241, 1996.

[6] F. Poitiers, T. Bouaouiche and M. Machmoum, "Advanced control of a doubly fed induction generator for wind energy conversion," *Electric Power Systems Research*, vol. 79, no. 7, pp. 1085–1096, 2009.

[7] M. El Azzaoui and H. Mahmoudi, "Fuzzy-PI control of a doubly fed induction generator-based wind power system," *International Journal of Automation and Control*, vol. 11, no. 1, pp. 54–66, 2017.

[8] M. M. Alhato and S. Bouallègue, "Thermal exchange optimization based control of a doubly fed induction generator in wind energy conversion system," *Indonesian Journal of Electrical Engineering and Computer Science*, vol. 20, no. 3, pp. 1–8, 2020.

[9] D. Zhou and F. Blaabjerg, "Bandwidth oriented proportional-integral controller design for back-to-back power converters in DFIG wind turbine system," *IET Renewable Power Generation*, vol. 11, no. 7, pp. 941–951, 2017.

[10] D. Horla and T. Sadalla, "Optimal tuning of fractional-order controllers based on Fibonacci-search method," *ISA Transactions*, vol. 104, no. 1, pp. 287–298, 2020.

[11] C. Zhao, D. Xue and Y. Q. Chen, "A fractional order PID tuning algorithm for a class of fractional order plants," in *Proc. of the IEEE Int. Conf. Mechatronics and Automation*, Niagara Falls, Ont., Canada, pp. 216–221, 2005.

[12] C. Viveiros, R. Melicio, J. Igreja and V. M. F. Mendes, "Performance assessment of a wind energy conversion system using a hierarchical controller structure," *Energy Conversion and Management*, vol. 93, no. 1, pp. 40–48, 2015.

[13] M. Hosseinabadi and H. Rastegar, "DFIG based wind turbines behavior improvement during wind variations using fractional order control systems," *Iranian Journal of Electrical and Electronic Engineering*, vol. 10, no. 4, pp. 314–323, 2014.

[14] H. Mahvash, S. A. Taher, M. Rahimi and M. Shahidehpour, "DFIG performance improvement in grid connected mode by using fractional order [PI] controller," *International Journal of Electrical Power & Energy Systems*, vol. 96, no. 1, pp. 398–411, 2018.

[15] M. M. Alhato and S. Bouallègue, "Whale optimization algorithm for active damping of LCL-filter-based grid-connected converters," *International Journal of Renewable Energy Research*, vol. 9, no. 2, pp. 986–996, 2019.

[16] Y. Liu, X. Yan, F. Yan, Z. Xu and W. Shang, "Sliding-mode PID control of UAV based on particle swarm parameter tuning," *Computers Materials & Continua*, vol. 63, no. 1, pp. 469–487, 2020.

[17] O. Mohamed Abdalla, H. Rezk and E. M. Ahmed, "Wind driven optimization algorithm based global MPPT for PV system under non-uniform solar irradiance," *Solar Energy*, vol. 180, no. 1, pp. 429–444, 2019.

[18] A. Assiri, "Anomaly classification using genetic algorithm-based random forest model for network attack detection," *Computers Materials & Continua*, vol. 66, no. 1, pp. 767–778, 2021.

[19] W. Zhao, Z. Zhang and L. Wang, "Manta ray foraging optimization: An effective bio-inspired optimizer for engineering applications," *Engineering Applications of Artificial Intelligence*, vol. 87, no. 1, pp. 1–25, 2020.

[20] I. Podlubny, "Fractional-order systems and PIλDμ controllers," *IEEE Transactions on Automatic Control*, vol. 44, no. 1, pp. 208–214, 1999.

[21] H. S. Li, Y. Luo and Y. Q. Chen, "A fractional order proportional and derivative (FOPD) motion controller: Tuning rule and experiments," *IEEE Transactions on Control Systems Technology*, vol. 18, no. 2, pp. 516–520, 2009.